17th World Conference on Earthquake Engineering, 17WCEE
Sendai, Japan - September 13th to 18th 2020

INFLUENCE OF AXIAL LOAD RATIO AND BOUNDARY ELEMENT ON DRIFT CAPACITY OF T-SHAPED STRUCTURAL WALLS

WJ. Zhang[(1)], Ch. Liu[(2)], JR. Qian[(3)]

[(1)] *Professor, College of Architecture and Civil Engineering, Beijing University of Technology,China,zhangweijing@sina.com*
[(2)] *Graduate student, College of Architecture and Civil Engineering, Beijing University of Technology, China, liuchao2802@163.com*
[(3)] *Professor, Department of Civil Engineering, Tsinghua University, China, qianjr@mail.tsinghua.edu.cn*

Abstract

The influence of axial load ratio, configuration and volumetric ratio of transverse reinforcement of wall boundary element on reinforced concrete T-shaped structural walls is studied through quasi-static test. Four slender reinforced concrete shear walls with T-shaped cross sections were tested under constant axial and reversed cyclic loads. Among the four specimens, the design axial load ratio of two specimens was 0.4 and that of the other two specimens was 0.55. At the flange region, no boundary elements were provided for three of the specimens, and boundary element was provided for the other specimen. At the free end of the web, opposite of the flange, boundary element with different lengths and different quantities of transverse reinforcement was provided for each specimen. The test results show that the failure modes of all the specimens were flexure-compression, crushing of core concrete and buckling of longitudinal reinforcement at the boundary elements of the free edge of the web occurred, some of the longitudinal reinforcement in the boundary element fractured, however, the intersection of the web and the flange did not undergo damage, and only minor spalling of concrete cover at both ends of the flange was observed. The lateral force versus top displacement hysteresis curve of the specimen is relatively full. When the web is in compression, for specimens with the same axial load ratio, the drift capacity increases with the increase of the length of the boundary element at the free end of the web and the increase of the volumetric ratio of boundary transverse reinforcement at the same time, and for the specimens with different axial load ratios, in order to achieve similar drift capacity, the specimens with high axial ratios require longer length of boundary element and tighter spacing of transverse reinforcement at boundary element at the free end of the web. For the flange in compression, the specimens with different axial load ratios and without boundary element at the flange region have large drift capacity, whereas specimen with axial load ratio of 0.55 can increase the drift capacity when boundary element was provided at the flange region.

Keywords: T-shaped structural walls; axial load ratio; boundary element; drift capacity; quasi-static test

1. Introduction

Reinforced concrete structural walls are used commonly as the lateral-load resisting system due to their high in-plane strength and stiffness. Due to the needs of architectural functions, a large number of shear walls in practical projects are shear walls with flanges. Due to the joint action of flanges and webs, seismic behavior of such combined section shear walls is relatively complex. Although a number of experimental studies have been conducted on flanged shear walls[1-6], in many cases, the experimental studies are under low axial load level. In addition, the length and construction of boundary element are mostly configured according to the code requirements. In this paper, two T-shaped shear wall specimens with design axial load ratio of 0.4 and two T-shaped shear wall specimens with design axial load ratio of 0.55 were designed to yield in flexure, and quasi-static tests were conducted to study the influence of axial load level, the length and volumetric ratio of transverse reinforcement in boundary element at the free end of web, and whether boundary element was set at the flange end on the deformation capacity of T-shaped shear walls.

2. Experimental program

2.1 Specimen design

Four reinforced concrete structural wall specimens with aspect ratio of 2.2(TW1-TW4), subjected to combined constant axial load and reversed cyclic lateral loading, were designed and tested. Among them, the design axial load ratio of specimens TW1 and TW3 is 0.4, and the design axial load ratio of the other two specimens TW2 and TW4 is 0.55. All specimens were of the same size. Walls were 2840mm tall and 160mm thick, with web length of 1200mm and flange length of 600mm. The section size of the top beam was 700mm wide and 300mm tall; and the section size of the ground beam was 400mm wide and 600mm tall. The dimension of the specimen is shown in Fig.1, the reinforcement detailing of the wall is shown in Fig. 2, and the parameters of the specimen are shown in Table 1. Primary test variables included axial load ratio, length of boundary element, quantities of transverse reinforcement at the wall boundaries, and with or without boundary element at the flange region.

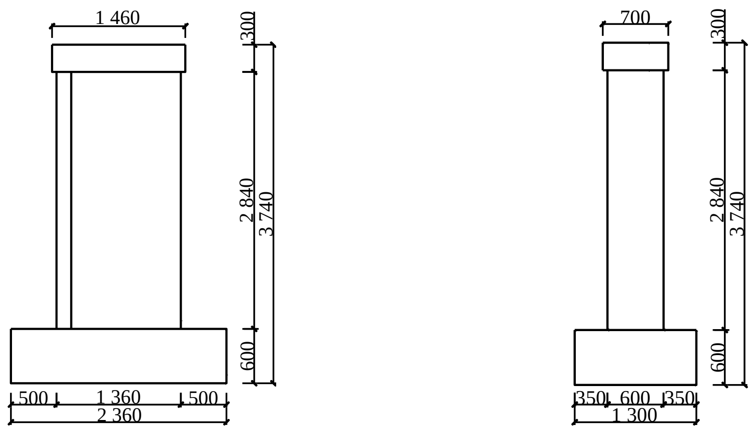

Fig. 1 –Geometry of specimen

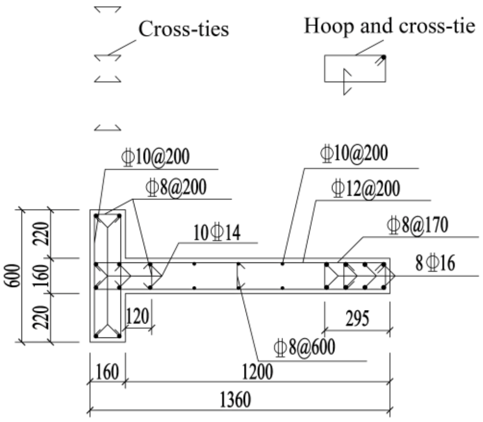

(a) Specimen TW1

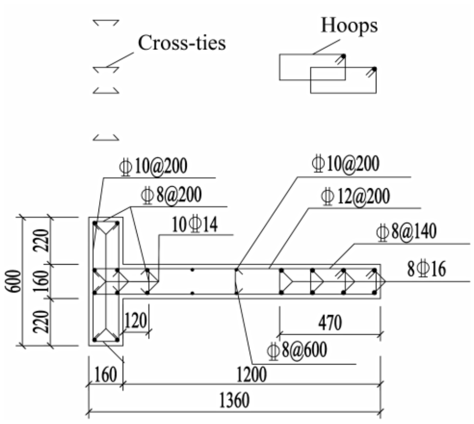

(b) Specimen TW2

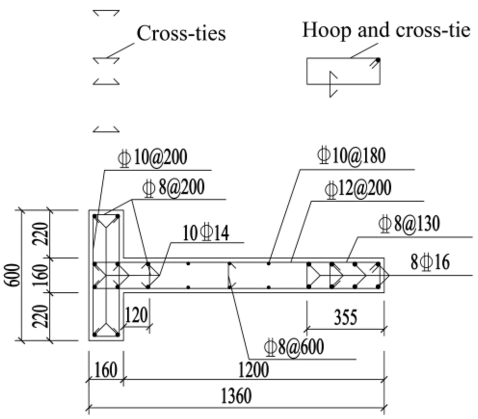

(c) Specimen TW3

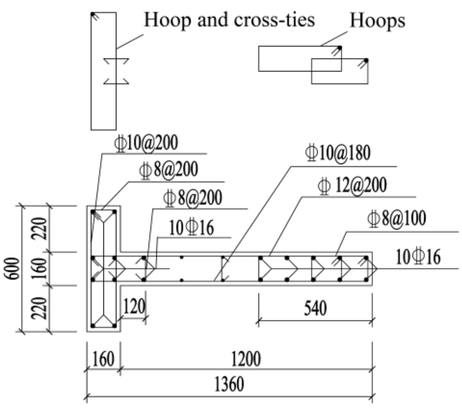

(d) Specimen TW4

Fig. 2 – Reinforcing details of the specimens

Table 1– Wall specimen attributes

Specimen ID	**Design axial load ratio**	**Applied axial load /kN**	**Test axial load ratio**	**Boundary element length at web end /mm**	**Length of flange /mm**	**Transverse reinforcement at web/ at flange**	**Volumetric ratio of transverse reinforcement**
TW1	0.40	1647	0.21	295	600	Φ8@170/	0.81%
TW2	0.55	2265	0.29	470	600	Φ8@140/	0.91%
TW3	0.40	1647	0.21	355	600	Φ8@130/	0.99%
TW4	0.55	2265	0.29	540	600	Φ8@100/ Φ 8@200	1.22% 0.59%

According to the Chinese code for seismic design of buildings [7], when the axial load ratio of shear wall at grade 1(7 or 8 degrees) is 0.4, the minimum length of boundary element at web edge of T shaped shear wall is 400 mm, and the minimum length of boundary element at flange and web interaction include no less than the flange thickness plus 600 mm along the flange direction, and no less than 300 mm along the web direction. For specimens TW1 and TW3 with a designed axial load ratio of 0.4, the length of boundary element at the free end of the web was less than the requirements of the specification, and no boundary element is provided at flange and web interaction. When the axial ratio was 0.55, the length of boundary element of TW2 at free end of the web was larger than the specification requirement, but no boundary element was set at the interaction of flange and web, whereas for the specimen TW4, the length of boundary element at the free end of the web was larger than the minimum requirement of the specification, but boundary element was set at the interaction of flange and web only along the direction of the flange.

2.2 Material properties

The design concrete compressive strength grade is C30 for walls, and the design concrete compressive strength grade is C50 for ground beam. Three standard cube blocks with side length of 150 mm are reserved for each specimen when pouring. The mean compressive strength of concrete cube is 35.9MPa ($f_{cu,m}$) before the test day, and the mean compressive strength is 27.3MPa ($f_{c,m}$=0.76$f_{cu,m}$). HRB400 steel was used for reinforcement and the measured mechanical properties for steel are provided in Table 3. In the Table, f_y and f_u represent the measured values of tensile yield strength and tensile ultimate strength of the reinforcement, respectively. The measured values are the average value of the three reinforcing bars, and d represents the diameter of the reinforcing bars. The yield strain of reinforcement is calculated from $\varepsilon_y = f_y/E_S$, and the elastic modulus (E_S) was assumed to be 2.0×10^{5}MPa.

Table 2 –Material properties of reinforcement

d/mm	*fy*/MPa	*fu*/MPa	$\varepsilon_y/10^{-6}$
8	412	603	2058
10	483	658	2416
12	428	582	2142
14	434	592	2172
16	442	604	2211

The quasi-static test method of applying reversed lateral load (lateral displacement) under constant vertical force is adopted in the test. The test loading device is shown in Fig.3. The specimen was fixed by the ground beam, and a 3000kN hydraulic jack was used to apply constant vertical load to the specimen, which was located at the centroid of the wall section. A hydraulic servo jack is used to apply the reversed load, and the horizontal load height is 2990mm away from the top surface of the ground beam. The test protocol consisted of load-controlled cycles, starting from 50kN, followed by displacement-controlled cycles after yielding. Cyclic loading is performed once for each load level and three times for each displacement level. When the positive lateral load decreases to less than 80% of the peak load or the specimen cannot bear the designed axial load, positive loading ends. After that, Cyclic loading is performed once for per stage in negative direction. The flange in tension and web in compression were defined as positive loading, and vice versa.
Instrumentation was used to measure loads, displacements and strains at critical locations. The LVDT layout is shown in Fig.4. Where, Sensors from D1 to D5 was used to measure total lateral displacement over the wall height. Sensor D1 was arranged in the middle line of the loading beam, 2990mm above the wall-foundation intersection. Sensor D6 was used to measure the sliding deformation of the base block; Sensors D7 and D8 were used to measure the uplift of ground beams. The measurement results show that there is no uplift or sliding during the test.

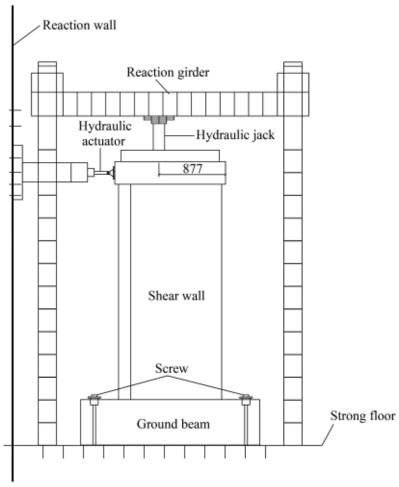

Fig. 3 – Schematic test setup

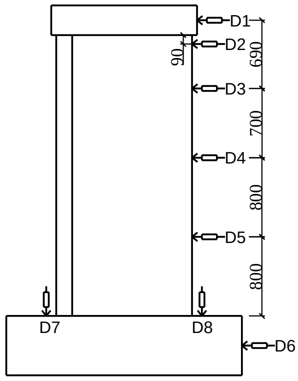

Fig. 4 – LVDT configuration

3. Experimental results

3.1 Progression of damage

Taking the specimen TW1 with an axial load ratio of 0.4 and TW3 with an axial load ratio of 0.55 as examples, the failure process of the specimen was introduced.

For specimen TW1, horizontal cracking initiated at the flange side and the web end at the base of specimen under lateral load of 250kN (0.18% drift). At 0.5% drift, more horizontal cracks developed at the lower heights of outer face of the flange, some existing cracks extended throughout the full length of flange, and the horizontal cracks at the web end became more inclined as they extended into the inner of the web to form diagonal cracks. At 1.1% drift, the concrete cover was loosened but not detached from the wall at the toe of the web end. At 1.3% drift, the maximum crack width on the flange was 3mm, and the maximum inclined crack width on the web was 2.5mm. Cover spalling occurred at the base of the web end, and six edge boundary bars were exposed, among which three were severely buckled. At 1.6% drift, concrete cover at web boundary from the wall-foundation interface to a height of approximately 500mm had completely spalled, core concrete of boundary element crushed, and the lateral load decreased to 75% of the peak load. During the second cycle to 1.6% drift in the negative direction, one longitudinal bar at the free end of the web fractured; during the third cycle to 1.6% drift in the positive direction, the axial load dropped sharply and positive loading was stopped. During the third cycle to 1.6% drift in the negative direction, two longitudinal bars at the free end of the web fractured. After that, the negative loading repeated once for each level. At 1.9% drift, two edge boundary bars at free end of the web fractured. At 2.1% drift, minor concrete cover at the toe of flange detached from the wall, and fracture of one longitudinal bar in boundary element at free end of web was observed, the wall lateral capacity decreased to 67% of the peak load, and significant loss of axial load-carrying capacity occurred, the test was stopped.

For the specimen TW3, horizontal cracks first occurred at the flange side and the web end at the bottom of wall under load of 150kN. When lateral load was 250kN, short horizontal cracks occurred on the outer face of flange. At 0.4% drift, horizontal cracks of flange increased significantly, some existing cracks continued to extend to the full length of flange, and horizontal and inclined cracks developed on the web. At 1% drift, cover spalling initiated at the bottom of the web end. At 1.6% drift, extensive cover spalling at the base of web end was observed, and two longitudinal bars on the outermost side of the boundary element were exposed and buckled. At 1.8% drift, minor spalling of cover concrete at flange edges occurred, whereas extensive cover spalling within region of 1000 mm from free edge of the web and a height of 400 mm above the wall-foundation interface occurred, the core concrete in boundary element crushed, the lateral load dropped to 78% of the peak load, under the third cycle loading in positive direction, eight longitudinal bars and two vertical distributed bars in boundary element were exposed and buckled, due to unable to maintain the vertical load, positive loading was stopped. During the third cycle in negative direction, fracture of two edge boundary bars was observed; after that, the negative loading repeated once for each level. At 2.0% drift, one more longitudinal reinforcement in boundary element at free end of web fractured. At 2.6% drift, transverse reinforcement of boundary element at free end of web fractured, and the lateral load dropped to 72% of the peak load, the test was stopped.

Fig. 5 shows the walls at the end of the test. It can be seen that: extensive cover spalling at the base of the web end was observed in the region of approximately 2/3 of wall length, the core concrete of boundary element crushed, the longitudinal and vertical distributed reinforcement in boundary element severely buckled, some of the longitudinal reinforcement and transverse reinforcement in boundary element fractured. Concrete cover slightly spalled at the toe of flange for specimen TW1, whereas some of the longitudinal bars at the toe of flange for specimens TW2~TW4 were exposed. The failure mode of the specimen is flexure-compression.

(a) Specimen TW1 (b) Specimen TW2

(c) SpecimenTW3 (d) Specimen TW4

Fig. 5 –Specimens after the test

3.2 Lateral load versus top displacement

The measured lateral load versus the top displacement for the four specimens are plotted in Fig. 6, and the skeleton curves are shown in Fig.7. The top horizontal displacement is the displacement measured at the measuring point D1, which is 2990 mm above the wall-foundation interface. It can be seen from Fig. 6 and Fig.7 that before yielding, there was almost no residual deformation of the specimen after unloading, and it was in the elastic stage. After the specimen yielded, with the increase of horizontal displacement and cycle times, the hysteresis curve gradually pinched, the hysteresis ring area increased, and the residual deformation increased after unloading. The hysteretic curves were relatively full and showed good energy dissipation capacity for all walls.

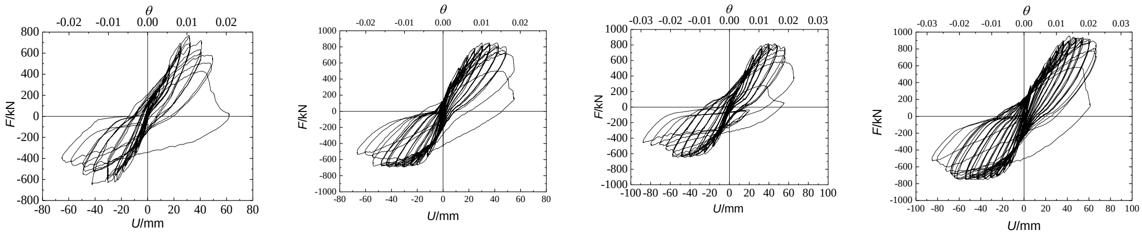

(a) Specimen TW1 (b) Specimen TW2 (c) SpecimenTW3 (d) Specimen TW4

Fig. 6 – Lateral load versus top displacement for specimens

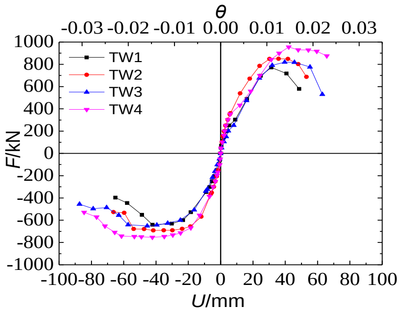

Fig. 7 – Comparison of skeleton curves

3.3 Lateral load capacity

Table 3 shows the load capacity of different damage states of the specimen, in which F_c, F_y and F_p represent the cracking load, nominal yielding load and peak load of the specimen, respectively. The first visible crack on the wall is defined the crack point; the nominal yielding point was determined by the lateral force-displacement skeleton curve at the top of the specimen using geometric drawing method. The point at which the lateral load reaches its maximum is the peak point. F_m in Table 3 is the lateral force corresponding to the compressive bending capacity of shear wall calculated in accordance with the current code of concrete structure [8]. In the calculation, the measured yield strength of steel bar is taken, and the mean value of axial compressive strength of concrete is 27.3Mpa. In Table 3, "+" represents positive loading, for the case with flange in tension, and "-" represents negative loading, i.e., for the case with flange in compression. The measured values of the peak carrying capacity of walls are from 1.03 to 1.30 times of the calculated values. The peak load capacity of the specimens under positive loading is from 1.20 to1.44 times that under negative loading, and the wall load capacity is higher for the flange in tension.

Table 3 –Lateral loads for different damage states

specimen ID	**Loading direction**	**F_c/kN**	**F_y/kN**	**F_p/kN**	**F_m/kN**	**F_p/F_m**
TW1	+	249.9	523.1	771.1	635.2	1.21
	-	250.9	439.5	640.8	543.7	1.18
TW2	+	302.4	614.2	850.0	701.5	1.21
	-	299.9	571.9	692.0	624.8	1.11

TW3	+	202.0	603.9	819.2	633.7	1.29
	-	215.8	511.1	651.7	543.7	1.20
TW4	+	150.4	701.8	923.5	707.8	1.30
	-	160.9	512.6	643.1	624.8	1.03

3.4 Drift capacity

The cracking displacement U_c, nominal yielding displacement U_y, peak displacement U_p and ultimate displacement U_u of the specimens are shown in Table 4, and the corresponding drift ratio θ_c, θ_y, θ_p and θ_u are also listed in Table 4. Drift ratio is calculated by U/H, where, U is the lateral displacement of the top of the specimen, H is the height of the measuring point(2990mm).The ultimate displacement is the corresponding lateral displacement when the lateral load of the specimen drops to 85% of the peak lateral load.

It can be seen from Table 4 that the ultimate drift ratio for the case flange in compression (displacement is negative) is 10%~14% larger than that under web in compression (displacement is positive). When the webs were in compression, for specimens TW1 and TW3 with axial load ratios of 0.4, the ultimate drift ratio of TW1 was 1.5%, and the ultimate drift ratio of TW3 with longer boundary element length and larger volumetric ratio of transverse reinforcement of the web was 1.9%. Similarly, for specimens TW2 and TW4 with axial load ratios of 0.55, the ultimate drift ratio of TW2 was 1.7%, and the ultimate drift ratio of TW4 with longer boundary element and larger volumetric ratio of transverse reinforcement at web end was 2.2%. The results show that for the specimens with the same axial load ratio, the deformation capacity of the wall increases with the increase of the length of the boundary element at the web end and the increase of volumetric ratio of transverse reinforcement. For specimens with different axial load ratios, in order to achieve similar deformation capacity, specimens with a high axial load ratio require longer length of boundary element at the web end and larger amount of transverse reinforcement. When flanges were in compression, specimens TW1, TW2 and TW3 with no boundary element at the flange region had an ultimate drift ratio from 1.7% to 2.1%, all of which had large deformation capacity. For the specimen TW4 with a boundary element at the flange region and with an axial load ratio of 0.55, the ultimate drift ratio was 2.4%, and the deformation capacity was larger.

Table 4 – Drift capacity of specimens

specimen ID		**cracking**		**yielding**		**peak**		**ultimate**	
		U_c/mm	θ_c	U_y/mm	θ_y	U_p/mm	θ_p	U_u/mm	θ_u
TW1	+	5.25	0.18%	17.64	0.59%	31.32	1.1%	44.27	1.5%
	-	5.33	0.18%	13.82	0.46%	42.16	1.4%	49.38	1.7%
TW2	+	4.43	0.15%	15.45	0.52%	35.89	1.2%	51.60	1.7%
	-	4.18	0.14%	12.33	0.41%	41.66	1.4%	57.52	1.9%
TW3	+	4.76	0.16%	21.12	0.70%	39.62	1.3%	57.82	1.9%
	-	5.01	0.17%	16.62	0.56%	45.39	1.5%	63.14	2.1%
TW4	+	2.08	0.07%	19.04	0.64%	42.15	1.4%	65.72	2.2%
	-	1.76	0.06%	12.99	0.40%	42.26	1.4%	72.41	2.4%

3.5 Stiffness degradation

The secant stiffness of the maximum displacement of each cycle under lateral load is defined as the equivalent stiffness K of the specimens. The equivalent stiffness degradation curves of specimen are shown in Fig.8. As can be seen from Fig.8, the equivalent stiffness of the specimen degrades rapidly before yielding, and slows down after yielding. The equivalent stiffness degradation of flange in compression is slower than that of web in compression. The initial equivalent stiffness of the flange in tension is greater than that of the web in tension.

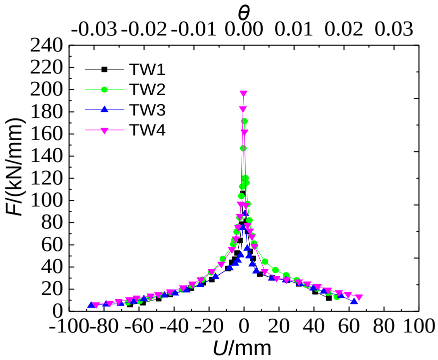

Fig. 8 –Stiffness degradation curves

4. Conclusions

The following conclusions can be obtained through the quasi-static test of four T-shaped shear wall specimens with high axial ratio, different boundary element lengths and configurations:

(1) The failure mode of the specimen is flexure-compression. Concrete at the free end of web crushed, boundary longitudinal bars buckled and some of them fractured, concrete cover on both sides of the flange bottom slightly spalled. For the specimen that boundary element not set as required by the specification at the flange region, no damage was observed at the web-flange intersection.

(2) When the flange is in tension, the lateral load capacity of the wall is higher, while when the flange is in compression, the deformation capacity is larger and the equivalent stiffness degradation is slower.

(3) When the web is in compression, for the specimens with same axial load ratio, increase the length of boundary element at web edge, and at the same time increase the volumetric ratio of transverse reinforcement, the deformation capacity increases; for the specimens with different axial load ratio, to achieve similar deformation capacity, the specimen with high axial load ratio requires longer length of the boundary element at web edge and larger volumetric ratio of transverse reinforcement.

(4) When the flange is in compression, the specimens with different axial load ratio and without boundary element at the flange region have large deformation capacity. For specimens with high axial load ratio, boundary element was set at the flange region can increase its deformation capacity.

References

[1] Paulay T, Priestley MJN,Synge AJ (1982): Ductility in earthquake resisting squat shear walls. *ACI Struct J Proc*, **98**(4), 554-562.

[2] Hassan M, El-Tawil S (2003): Tension flange effect width in reinforced concrete shear walls. *ACI Struct J*, **100**(3), 349-356.

[3] Palermo D, Vecchio FJ (2002): Behavior of three-dimensional reinforced concrete shear walls. *ACI Struct J*, **99**(1), 81-89.

[4] Thomsen IV JH, Wallace JW (2004): Displacement-based design of slender reinforced concrete structural walls—experimental verification. *Journal of Structural Engineering*, **130**(4), 618-630.

[5] Fu JP, Wang JL, Bai ShL (2008): The seismic shear capacity of I-shaped and T-shaped reinforced concrete structural walls. *Journal of Chongqing Jianzhu University*, **30**(3), 21-26.

[6] Shi QX, Wang B, He WF, et al (2017): Experimental research on seismic behavior of reinforced concrete shear walls with flange. *Journal of building structures*. **38**(1):106-115.

[7] GB50011-2010(2010): *Code for seismic design of buildings*. Beijing: China Architecture & Building Press.

[8] GB50010-2010(2010): *Code for design of concrete structures*. Beijing: China Architecture & Building Press.